Research paper

Theoretical and experimental study of a new thiosulfonate derivative: Methyl trifluoromethanethiosulfonate, $CF_3SO_2SCH_3$. Conformational transferability in CX_3SO_2S-R compounds

J.E. Galván [a], E. Contreras Aguilar [b], M.E. Defonsi Lestard [a,1], M.E. Tuttolomondo [a], S.E. Ulic [b,c,1], A. Ben Altabef [a,*,1]

[a] INQUINOA-CONICET, Instituto de Química Física, Facultad de Bioquímica, Química y Farmacia, Universidad Nacional de Tucumán, San Lorenzo 456, T4000CAN, Tucumán, Argentina
[b] CEQUINOR, Departamento de Química, Facultad de Ciencias Exactas, Universidad Nacional de La Plata, C. C. 962, 1900 La Plata, Argentina
[c] Departamento de Ciencias Básicas, Universidad Nacional de Luján, Ruta 5 y 7, 6700 Luján, Buenos Aires, Argentina

ARTICLE INFO

ABSTRACT

Methyl trifluoromethanethiosulfonate, $CF_3SO_2SCH_3$, was synthesized and characterized by ^{13}C NMR, ^{19}F NMR, and vibrational spectroscopy. This structural study was supported by MP2 and DFT (B3LYP and MPW1PW91) calculations, which revealed a strong dependence of the theoretical structure on the polarization of the basis set. Theoretical data indicate that only one conformer, *gauche*, is predicted by rotating around the S–S bond. This conformational preference was studied using the total energy scheme and natural bond orbital partition scheme. These results evidence that electron delocalization and especially LP S → σ* C(1)-S interactions play an interesting role in the reactivity-structure connection of oxoesters and thioesters.

Gas and liquid infrared and liquid Raman spectra were recorded and assigned. The experimental vibrational data along with theoretical force constants (B3LYP) were used to define a scaled quantum mechanical force field, which enabled the reproduction of the measured frequencies with a final root-mean-square deviation of 8.06 cm^{-1}.

© 2016 Elsevier B.V. All rights reserved.

1. Introduction

Thiosulfonates (CX_3SO_2S-R) are important in organic chemistry and biochemistry [1] since the relationship between their structural features and conformational preferences applications in cancer research and they act as antiviral agents.

Methanethiosulfonate reagents were first developed as tools to probe the structures and functions of proteins, particularly membrane proteins like ion channels [2]. The reagents react selectively and rapidly with thiols (sulfhydryls) to form disulfide bonds and, therefore, are highly efficient labeling agents for cysteine residues in proteins [3]. Papers have been published describing applications of methanethiosulfonates in cancer research [1] and as chemopreventive agents for liver neoplasia when administered in combination with Phenobarbital [4], a bio-antimutagen reagent [5].

The CX_3SO_2S-R group can interact with different intracellular proteins such as enzymes or receptors [6]. R-methanethiosulfonate (MTS) compounds are useful reagents to detect the thiol group present in cysteine residues of proteins by forming disulfide bonds [5] that are appropriate agents to characterize the structure and function of proteins.

The structural and conformational properties of $CH_3SO_2SCH_3$ [7] (MMTS) have already been studied in this laboratory. The gas-phase electron diffraction analysis of MMTS resulted in *gauche* structures with a CSSC dihedral angle of 80.1° and, when we extended our investigation to the $CF_3SO_2SCF_3$ [8] molecule, the structural results predicted a *gauche* conformation (92.9°) as the most stable form.

The knowledge of physicochemical properties and reaction sites of bioactive compounds in theoretical studies is essential to gain a deeper insight into their properties and thus help in the design of new drugs with therapeutic effects. Hence, MMTS interaction with DPPC bilayers was studied by a combination of Fourier transform infrared (FTIR) and SERS spectroscopy with MD (Molecular Dynamics) simulations and quantum calculations, comparing the

* Corresponding author at: INQUINOA-CONICET, Instituto de Química Física, Facultad de Bioquímica, Química y Farmacia, Universidad Nacional de Tucumán, San Lorenzo 456, T4000CAN, San Miguel de Tucumán, Argentina.
E-mail address: altabef@fbqf.unt.edu.ar (A. Ben Altabef).
[1] Member of the Research Career of CONICET.

simulated and experimental FTIR and Raman spectra [9,10]. Dipalmitoylphosphatidylcholine (DPPC) and MMTS would provide a better knowledge of their probable interaction.

Because of the extensive and varied field of application of this compound, we studied a new thiosulfonate derivative: Methyl trifluoromethanethiosulfonate, $CF_3SO_2SCH_3$, synthesized according to reported literature [11]. Its structure was determined by theoretical calculations and compared with related sulfonates [7,8,12–14]. The barrier to internal rotation about the S—S bond was calculated using an assortment of computational approaches (both *ab initio* and DFT), and fitted to a sixfold Fourier-type expansion. The nature of the potential function was analyzed and the preferred conformation of the molecule was assessed with this methodology. The study was complemented by natural bond orbital (NBO) analysis to determine the presence of hyperconjugative interactions which favored a particular conformation. Additionally, infrared and Raman spectra were recorded and complemented by quantum chemical calculations to obtain an optimized geometry and the corresponding frequencies of the normal modes of vibration.

2. Materials and methods

2.1. Instrumentation

2.1.1. Infrared and Raman spectroscopy

Infrared spectra of $CF_3SO_2SCH_3$ in the gas and liquid phases were recorded with a resolution of 2 cm^{-1} in the $4000–400 \text{ cm}^{-1}$ range at room temperature using a LUMEX Infra LUM FT-02 spectrometer. An IR glass cell (200 mm optical path length) with 0.5 mm thick Si windows was used to obtain gas phase spectra, whereas AgCl windows were employed for the liquid IR spectra. Raman spectra of the liquid at room temperature were obtained with a Thermo Scientific spectrometer (spectral resolution 4 cm^{-1}) and the 780 nm radiation line of a diode laser was used for excitation. The liquid sample was handled in flame- sealed capillaries (4 mm o. d.).

2.1.2. NMR spectra

The ^1H and ^{13}C NMR spectra were recorded at 25 °C on a Bruker Avance 200 spectrometer. The sample contained in a 4 mm flame-sealed capillary was introduced into a 5 mm NMR tube, using the residual signals of d$_6$-DMSO as external reference. Chemical shifts (δ) are given in parts per million (ppm), coupling constants (J) are reported in Hz and ~~the~~ multiplicity is signalized as: *s* (singlet) and *d* (doublet).

2.1.3. UV–visible spectroscopy

The UV–visible spectra of the title compound were recorded on a UV–visible Hewlett-Packard 8454-A diode array spectrophotometer at 2.0 nm spectral bandwidth, using a quartz cell (100 mm optical path length). Measurements were carried out in the spectral region from 200 to 700 nm.

3. Computational details

The Gaussian 03 [15] set of programs was used to carry out the *ab initio* and DFT calculations. Full optimizations were performed with standard gradient techniques at the MP2 [16] and DFT levels of theory. Three types of basis sets were employed: Pople's 6-31G (d), 6-311(3df), 6-311+(d) and 6-311++G(d,p) [17–22] basis sets were used as examples of small and large bases developed for molecular orbital (MO) calculations. Furthermore, Dunning's correlation consistent basis set of medium size, cc-pVDZ [23], was also essayed. Becke's hybrid exchange B3 [24] was the exchange functional, and the Lee–Yang–Parr non-local functional, LYP [25] was

employed for correlation. Also, the mPW1PW91 model was used as a modified Perdew-Wang exchange functional and Perdew-Wang 91 correlation [26] in order to assess the effect of the different HF exchange percentages (20% and 25%, respectively) on the molecular structure and vibrational properties.

The nature of the stationary points was checked through the vibrational wavenumbers, calculated from the analytical second derivatives of energy.

The study of the rotational barrier for the C—S—S—C torsion in terms of hyperconjugative, steric and electrostatic interactions provided an insight into the reasons for the relative stability of the *gauche* conformer. The potential energy curve for the corresponding torsion angle was calculated in 5° steps in the 0–180° range, allowing all other geometrical parameters to relax. The energy profiles were fitted to a sixth-order Fourier expansion [27].

$$V(\theta) = \sum_{i=1}^{6} \frac{1}{2} V_{iN} \left(1 - \cos iN\theta\right) \tag{1}$$

where N, the symmetry number, is equal to 1. No contributions to torsional energies from zero-point energy were taken into account.

Natural bond orbital calculations were performed at the B3LYP/6-311G (3df) level using the NBO 3.0 [28] code as implemented in the Gaussian 03 package. The force constant calculations for $CF_3SO_2SCH_3$ including a force field transformation, scaling and determination of the potential energy distribution, was performed with the FCARTP program [29].

Electronic transitions were calculated within the framework of the Time-Dependent Density Functional Theory [30] at the-B3LYP/6-311++G(d,p) level.

4. Synthesis, physical properties and spectroscopic characterization

4.1. Synthesis

Methyl trifluoromethanethiosulfonate, $CF_3SO_2SCH_3$, was obtained by reaction of CH_3SCl and $Zn(CF_3SO_2)_2$ based on the a reported synthesis [11] with some modifications. CH_3SCl (5 mmol) was condensed, through a vacuum line, into a flask containing Zn $(CF_3SO_2)_2$ (2 mmol). The reaction mixture was cooled at −20 °C and stirred for 24 h. The product was isolated by trap to trap distillation, keeping the traps at −65, −100 and −196 °C. $CF_3SO_2SCH_3$ was retained at −65 °C, as a colorless liquid. The purity of the product was checked by FT-IR spectroscopy. As methyl trifluoromethanesulfonate is quite sensitive to atmospheric conditions and temperature, the pure compound was stored in flame-sealed glass ampoules under liquid nitrogen in a Dewar vessel.

^1H NMR (200 MHz, DMSO) $\delta = 2.34$ (s, 3H, CH_3). ^{13}C NMR (50 MHz, DMSO) $\delta = 119.27$ (d, $J = 327.0$ Hz, CF_3), 17.92, CH_3(s). ^1H NMR (200 MHz, DMSO) $\delta = 2.34$ (s, 3H, CH_3). ^{13}C NMR (50 MHz, DMSO) $\delta = 119.27$ (d, $J = 327.0$ Hz, CF_3), 17.92, CH_3(s) (see Table S1).

4.2. Structural results

No theoretical or experimental structures were available for $CF_3SO_2SCH_3$, but our research group studied several methanesulfonic acid derivatives, where mostly fluorinated ones exhibit a gauche conformation. Thus, it was possible to predict that the conformations with dihedral angle (C—S—Y—C, Y = S,O) ranging from 80 to 135° would be the most stable structures for the studied compounds ($CF_3SO_2OCH_3$ [12], $CF_3SO_2OCF_3$ [13], $CH_3SO_2SCH_3$ [7], $CF_3SO_2SCF_3$ [8], $CCl_3SO_2OCH_2CF_3$ [31], $CF_3SO_2OCH_2CH_3$ [32], $CF_3SO_2OCH_2CF_3$ [33] and $CF_3SO_2OCCl_3$ [34]).

In order to gain some insight into the rotational barrier of this compound, the potential energy of the C—S—S—C torsion was calculated at the MP2, B3LYP and MPW1PW91 levels, using the 6-311G (3dfd) basis set (Fig. S1). A good agreement was found between the MP2 and DFT methods, both predicting two minima and mirror images with S(5)—C(6) bond (for atom numbering see Fig. 1) approximately eclipsing one of the S=O bonds.

The *gauche* conformation, with a C-S-S-C dihedral angle of about 82.89° (MP2/6-311++G(3df)) is shown in Fig. 2, and the calculated energies are reported in Table S2.

All geometry optimizations (MP2 and DFT with different basis sets) predicted the *gauche* conformation as the preferred one. Calculated geometric parameters for $CF_3SO_2SCH_3$, theoretical values obtained for $CF_3SO_2SCF_3$ [8] and computed and experimental (GED) values of $CH_3SO_2SCH_3$ [7] are compared in Table 1.

As found for related compounds [7,8,12–14,34], inclusion of extra polarization functions (beyond a single d function) was necessary to predict accurately the bond lengths in this type of molecule.

As shown in Table 1, the bond length distance of $C-S(SO_2)$ and C-S(S) decreased with decreasing electronegativity of the group CX_3 (X = H,F) while the opposite behavior was observed for the S=O bond distance.

The S—S bond was the most sensitive parameter to changes in electronegativity; the bond length underwent a different behavior. The S—S bond distance was shorter for $CF_3SO_2SCH_3$ in comparison with the other two thioesters. This fact could be explained by the electronegativity difference between the CX_3 groups (X = F, H) around the S—S bond, which affects the value of local dipoles and electron delocalization.

The decomposition of the total energy function and the analysis of the different V_i terms were carried out to determine why most sulfonates prefer the gauche conformation.

As previously shown, it is an effective method of analyzing the stabilization of different conformations in molecular systems [34–38]. Table S3 lists the six V_i terms calculated for $CF_3SO_2SCF_3$, $CF_3SO_2SCH_3$ and $CH_3SO_2SCH_3$ using the B3LYP/6-31G(d) basis set. The large values of V_1 and V_2 were the main contributions to the rotational barrier with $V_2 > V_1 > V_3$. V_{4-6} were less significant when deconvoluting the potential energy curve.

Fig. 2 shows the Fourier decomposition for the potential energy function, calculated at the B3LYP/6-311G(3df) level for three different sulfonates. V_1 is large and negative, showing that there is a strong preference for an *anti* geometry.

As shown in Table S3, also in Fig. 2, the value of V_1 is greater in the fully methylated sulfonate, $CH_3SO_2SCH_3$. Taking into account the behavior of the dipole moment with the variation of the CSSC dihedral angle for sulfonates, greater changes of the dipole moment were found in $CH_3SO_2SCH_3$. This result is consistent with the electrostatic effects that influence the stability of the *anti* form, which is the most stable conformation for $CH_3SO_2SCH_3$.

This fact can be rationalized by considering the interactions between local dipoles through the SO_2Me group and through SMe. As shown in Fig. S2, the total dipole moment (μ) for the *anti* conformer is smaller than that for the *gauche* conformer. This indicates that for the *anti* conformer these local dipoles are opposite in direction, a fact consistent with the value for V_1 given by the Fourier analysis.

For all sulfonates the V_2 term is large and negative, which favors the gauche form over the *anti* conformer. This term is much larger in the fluorinated compounds. This fact was discussed in a previous work by Defonsi et al. [8], but it should be noted that the greatest value of V_2 occurs in $CF_3SO_2SCH_3$. This is because the difference in electronegativity between the CX_3 (X = H, F) groups and the *gauche* form favors the orbital overlapping, so that a greater electron delocalization is observed.
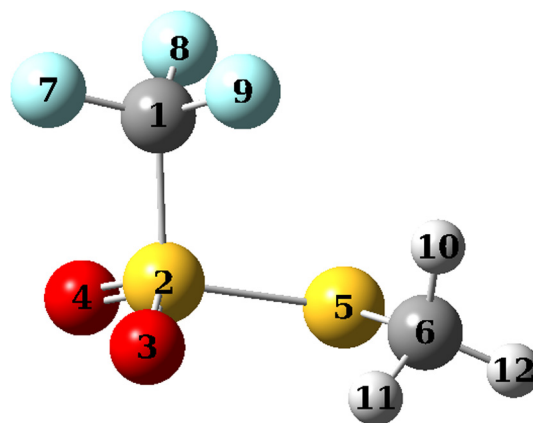

Fig. 1. Molecular structure of the *gauche* conformer of $CF_3SO_2SCH_3$ showing atom numbering.

The V_3 term is associated with adverse bond-bond eclipsing interactions, exhibiting a threefold periodicity for a torsion involving sp^3-hybridized sulfur atoms [37]. As V_1 term, V_3 also preferentially stabilizes the *anti* conformer, but the large and negative V_2 term favors the *gauche* form over the *anti* form.

4.3. Vibrational study

The main conformer of $CF_3SO_2SCH_3$ has C_1 symmetry and its 30 normal modes of vibration are active in IR and Raman. Representative spectra are shown in Fig. 3(a, b) (IR gas and SQM calculated spectra) and 4 (Raman liquid and SQM calculated spectra) while the frequencies of the observed spectral features are summarized in Table S4 and Fig. S3.

The DFT calculations reproduced the normal frequencies of vibration with the following RMSD (root mean square deviation) values for each basis set: 65.45 cm^{-1} for 6-31G(d), 54.96 cm^{-1} for 6-311G(3df), 57.86 cm^{-1} for 6-311++G(d,p) and 62.68 cm^{-1} for cc-pVdz (Fig. S4). Although the second and third basis sets reproduced the experimental frequencies somewhat better, the results obtained with 6-31G(d) basis set were used for the vibrational analysis in order to facilitate the comparison of the present results with those obtained earlier for related molecules. In fact, the combination B3LYP/6-31G(d) is being extensively used for vibrational calculations as a good compromise between economy of computational resources, accuracy and applicability to many-atoms systems [7,8,12–14,31–34]. The vibrational behavior of methanesulfonic acid derivatives was extensively studied by our group and the corresponding assignment for $CF_3SO_2SCH_3$ was performed based on these earlier works.

4.3.1. CH_3 modes

The three CH_3 stretching modes are located in the 3000 cm^{-1} region. Three bands can be observed in the gas spectrum at 3000, 2970 and 2926 cm^{-1} which are assigned to the antisymmetric and symmetric stretching modes. Taking into account the frequencies and assignments for the $CH_3SO_2SCH_3$ [7], the lowest frequency (2926 cm^{-1}) corresponds to the symmetric CH_3 stretching with an intense Raman counterpart at 2944 cm^{-1}, whereas the 3000–2970 cm^{-1} bands correspond to the antisymmetric CH_3 modes. The CH_3 bending modes should appear in the 1480–1400 cm^{-1} region. The very weak bands and shoulders that appear in the infrared and Raman spectra can be assigned to these modes, as detailed in Figs. 3(b) and 4. The relative ordering of these bending modes is well reproduced by calculations. The CH_3 rocking modes
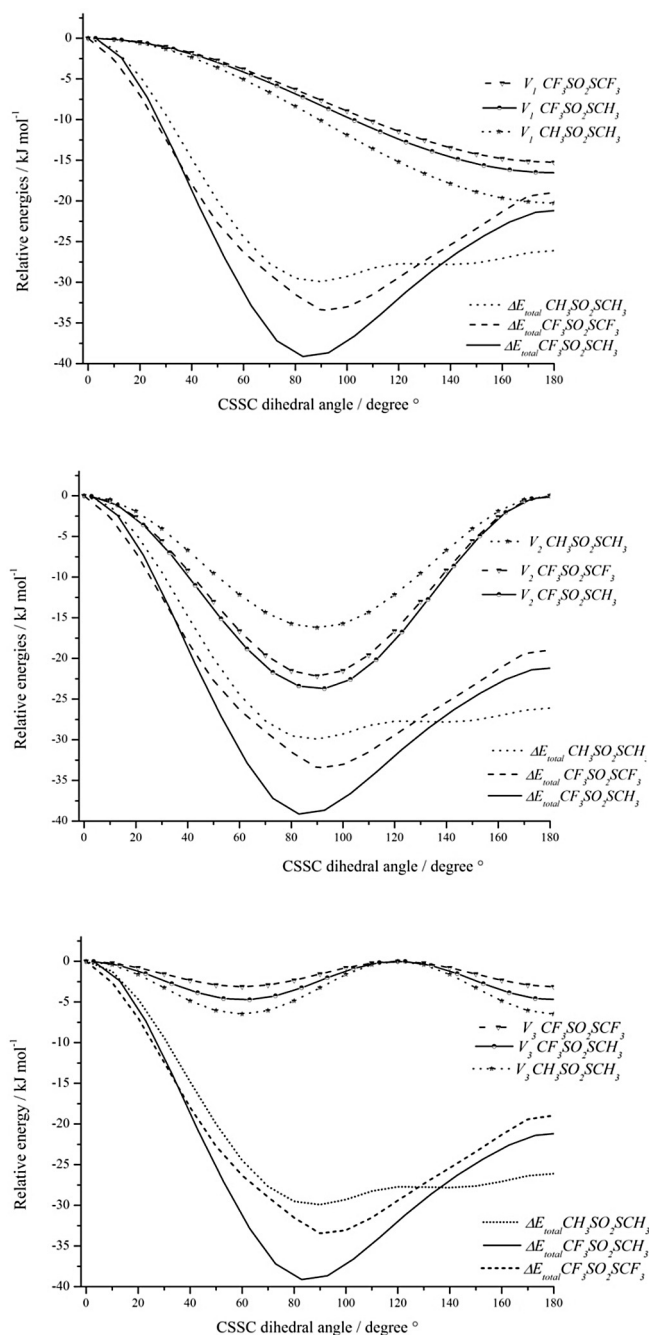
Fig. 2. Fourier decomposition of the potential function $V(\phi)$ for $CF_3SO_2SCF_3$ $CF_3SO_2SCH_3$ and $CH_3SO_2SCH_3$ at B3LYP/6-311G(3df) level.

are assigned at 963 and 951 cm^{-1} with a $\Delta\nu$ of 12 cm^{-1} which is well reproduced by theoretical calculations ($\Delta\nu$ = 10 cm^{-1}).

4.3.2. CF$_3$ modes

The band located at 1197 cm^{-1} in the Raman spectra of the liquid was assigned to the CF$_3$ symmetric stretching, while the very intense band at 1221 cm^{-1} (IR gas) corresponds to both antisymmetric stretching absorptions.

4.3.3. SO$_2$ modes

For the CF$_3$SO$_2$R derivatives, (R = F, OH, NH$_2$, OCH$_3$SCH$_3$,OCF$_3$, SCF$_3$) [7,8,12–14,34], the SO$_2$ antisymmetric and symmetric stretching modes appear in the region at 1467–1357 cm^{-1} and

at1157-1100 cm^{-1}, respectively. Two strong infrared bands are observed at 1400 and 1124 cm^{-1}for the CF$_3$SO$_2$SCH$_3$, and they are assigned to the SO$_2$ antisymmetric and symmetric stretching modes, respectively. In covalent sulfonates, the SO$_2$ stretching modes are very sensitive to changes in the electronegativity of the substituents. The increase in the electronegativity of the CX$_3$ group causes a greater separation between the antisymmetric and symmetric stretching bands. This behavior, also observed experimentally, agrees with calculated data (Table 2).

4.3.4. Skeletal modes

The S—S stretching mode, which is strongly coupled with the bending and rocking modes of the CF$_3$ group, appears as a main component of the ν_{16} and ν_{21} modes which are associated with medium and strong Raman bands at 629 and 407 cm^{-1}, respectively. The same mode was attributed to CH$_3$SO$_2$SCH$_3$ [7] and CF$_3$SO$_2$SCF$_3$ [8] at 557 and 604 cm^{-1}, respectively. The C(1)—S(2) and S(5)—C(6) stretching modes are associated with the bands located at 371 and 690 cm^{-1}, respectively, in the Raman spectrum.

4.3.5. Electronic analysis

The experimental and calculated UV–visible spectra of methyl trifluoromethanethiosulfonate are presented in Fig. 5. Table 3 shows the main absorption bands correlated with the calculated values and a tentative assignment of the electronic transitions. Only the dominant transitions (f > 0.06) were used to assign the observed bands.

The main involved molecular orbitals are displayed in Fig. 6. The shoulder observed at 210 nm is mainly due to the contribution of one electron in transitions HOMO−1 → LUMO+2 and HOMO-4 → LUMO (Calc. 168 and 170 nm). It is originated by excitations from non-bonding orbitals of both oxygen atoms and the sulfur atom attached to the CH$_3$ group to some d character orbitals of the S atom of the SO$_2$ group.

The absorption at 252 nm is attributed principally to transitions from HOMO−1 → LUMO (Calc. 207 nm). This absorption is generated by transitions from non-bonding orbitals of both oxygen and one of the sulfur atoms to the σ^* orbital of the S—S single bond.

5. NBO analysis

The role of hyperconjugative interactions in the stabilization of the *gauche* conformer has been assessed using NBO analysis, where the hyperconjugation represents the transfer of an electron between a lone pair or bonding orbital and an antibonding orbital (Table 4).

Table 4 shows the most important hyperconjugative interactions at the B3LYP/6-31+G(d)for the *gauche* conformer of the CF$_3$SO$_2$SCH$_3$ and related molecules (CH$_3$SO$_2$SCH$_3$and CF$_3$SO$_2$SCF$_3$). Taking into account the different electronegativity of the CX$_3$ groups, it can be observed that by increasing electronegativity, the total hyperconjugative interactions are higher. The *gauche* form favors the orbital overlap and, with increasing electronegativity of CX$_3$ group, the interacting atoms have a positive charge which facilitates electron delocalization.

Fig. 7 displays the interaction of sulfur atom lone pairs (LP S) with a neighboring bond (XY) (anomeric effect) for thiocompounds with different electrostatic environments. X-SS-X compounds (X = F, Cl, CF$_3$, CH$_3$, FC(O)) [39–43] show that a higher electronegativity of X increases the anomeric effect (S···XY) and therefore the value of the υ S—S frequency.

However, this behavior is not observed in thiosulfonates where the presence of the SO$_2$ group causes an increase in electron density. The electronegativity difference between the CF$_3$ and CH$_3$

Table 1
Geometrical parameters for $CF_3SO_2SCF_3$, $CF_3SO_2SCH_3$ and $CH_3SO_2SCH_3$ calculated at the B3LYP/6-311 G(3df) level.

	$CF_3SO_2SCF_3$[a]	$CF_3SO_2SCH_3$[b]	$CH_3SO_2SCH_3$[c]	Experimental
Distances (pm)[d]				
C—S (SO₂)	188.8	188.1	179.0	178.46
S—S	211.9	208.4	211.1	207.47
C—S(S)	184.8	182.2	182.1	182.2
S=O	142.8	143.2	143.8	143.4
CX₃(SO₂)	132.3	132.7	108.8	108.86 (mean)
CX₃(S)	132.9	132.7	108.8	108.86 (mean)
Angles (°)				
C—S(SO₂)—S	103.1	103.9	104.9	102.8
C—S—S(SO₂)	102.1	101.1	100.7	100.3
O=S=O	123.8	123.0	121.5	121.0
Dihedral angle (°)				
CSSC	92.9	85.5	84.9	80.1

[a] Ref. [8].
[b] Ref. [this work].
[c] Ref. [7].
[d] X = F, H.
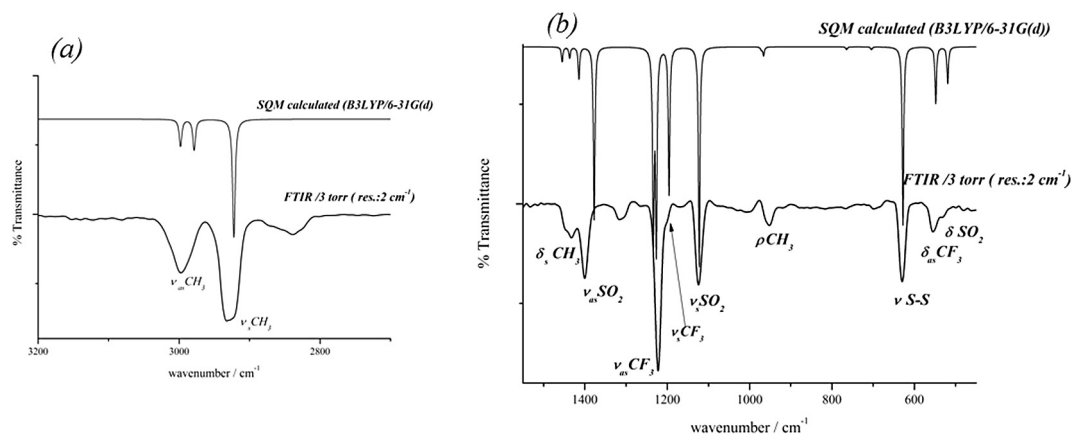
Fig. 3. Vibrational IR experimental (gas) and calculated spectra of $CF_3SO_2SCH_3$ between: (a) 3200–2800 cm^{-1} and (b) 1550–450 cm^{-1}.

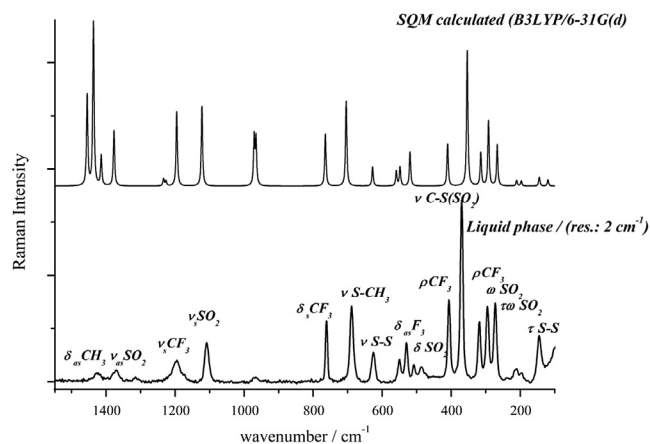**Fig. 4.** Raman experimental (liquid) and calculated spectra of $CF_3SO_2SCH_3$ between 1550 and 100 cm^{-1} at 2 cm^{-1} resolution.

Table 2
Δv between SO₂ stretching bands for different covalent sulfonates.

	$\Delta\upsilon$ calc.	$\Delta\upsilon$ exp.
CH₃SO₂SCH₃	196	171
CH₃SO₂OCH₃	201	178
CF₃SO₂SCH₃	237	262
CF₃SO₂OCH₃	261	276
CF₃SO₂OCCl₃	304	312
CF₃SO₂SCF₃	285	322
CF₃SO₂OCF₃	317	332

ample stabilization of the *gauche* form with a greater V_2 value between the anti and *gauche* forms for $CF_3SO_2SCH_3$ (Fig. 2); second, a higher anomeric effect (LP S → σ* C (1)–S(2)) produces a decreased σ*S—S occupancy (Table S5) decreasing its bond length and increasing υ S—S frequency.

6. Force constant calculations

The cartesian coordinate force field, as generated by the Gaussian program [15] at B3LYP/6-31G(d) level, was transformed with a set of non-redundant, natural coordinates defined in Table S6.

Such coordinates take into account the local symmetry around the C and S atoms and follow the proposals of Fogarassi et al.
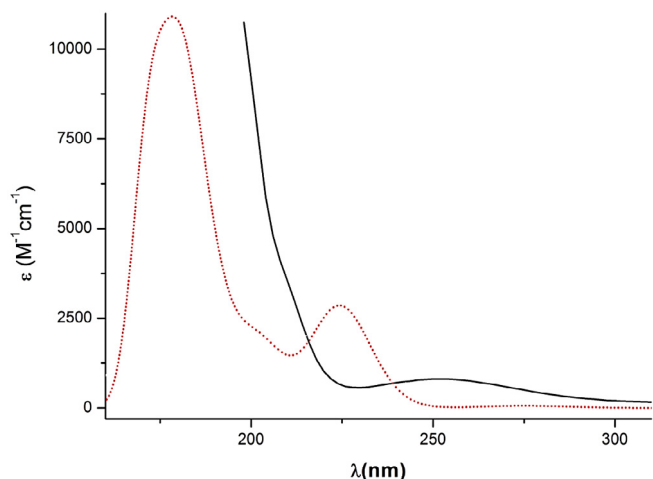
groups in $CF_3SO_2SCH_3$, favors the anomeric effect (LP S → σ* C (1)–S(2)) with respect to the $CF_3SO_2SCF_3$ and $CH_3SO_2SCH_3$; this is because the interacting atoms present in the $CF_3SO_2SCH_3$ in this delocalization have a positive charge that favors the interaction of free electron pairs of the S atom with the antibonding orbital C—S. This behavior has two important effects: first, there is an

Fig. 5. Experimental (full trace) and calculated (dashed trace) electronic spectra (B3LYP/6-311++G(d,p), of CF$_3$SO$_2$SCH$_3$ in gas phase (1 Torr) at room temperature.

Table 3
Observed electronic spectrum of CF$_3$SO$_2$SCH$_3$ along with calculated electronic transitions relevant for the assignments.

Experimental[a]	Calculated[b] (PBEPBE/6-311++G(d,p))	Assignment
	180 (0.089)	HOMO−1 → LUMO+2 (40%)
		HOMO−2 → LUMO+1 (23%)
210[c]	202 (0.023)	HOMO−4 → LUMO (56%)
		HOMO → LUMO+2 (29%)
252	225 (0.046)	HOMO−1 → LUMO (79%)

[a] Absorption maxima spectral positions are given in nm.
[b] Oscillator strengths of calculated transitions, shown in parenthesis, are in atomic units.
[c] Shoulder.

[44] The resulting force field was subsequently scaled using the scheme proposed by Pulay et al. [45] where the diagonal force

Table 4
Relevant hyperconjugative interactions (kJ mol^{-1}) for CF$_3$SO$_2$SCF$_3$, CF$_3$SO$_2$SCH$_3$ and CH$_3$SO$_2$SCH$_3$ calculated at the B3LYP/6-31+G(d) level.

	CF$_3$SO$_2$SCF$_3$	CF$_3$SO$_2$SCH$_3$	CH$_3$SO$_2$SCH$_3$
LP[a] S → σ* C−X[b](7,8,9)	3.30	3.30	3.89
LP[a] S → σ* C−X[b](10,11,12)	59.27	31.31	32.77
LP S → σ* C (1)−S(6)	19.31	23.66	14.30
∑ LP S → σ* S (6)=O(4,5)	11.16	15.88	13.08
LPO (3) → σ* S (6)=O(5)	97.77	94.34	96.01
LPO (4) → σ* S (6)=O(4)	99.69	97.81	101.03
∑ LP O (3, 4) → σ* S−S	267.31	240.31	249.00
∑ LP X(7,10) → σ* S−S	3.10	–	–
∑ LP X(7,8,9) → σ* C(1)−S(2)	148.89	129.50	–
∑ LP X(10, 11, 12) → σ* S(5)—C (6)	63.33	–	–
Total	773.13	636.11	510.08

[a] LP denotes electron lone pair in the atom (for atom numbering see Fig. 2).
[b] X = F, H.

constants were multiplied by a set of scale factors k_i, k_j, … and the corresponding interaction constants multiplied by $(k_i \times k_j)^{1/2}$. The initial scale factors were defined with the values used before for the sulfonates calculated previously [7,8,12–14,31–34]. In the adjustment, the same weight was assigned to all vibrational bands except for those missing or showing uncertain frequencies; in these cases a value of zero was used. No empirical correction of the theoretical geometry was used. The potential-energy distribution matrix was calculated with the resulting scaled quantum mechanics (SQM) force field. The final RMSD and potential-energy distribution are presented in Table S4.

The SQM force field (Table S7, Supporting Information) was used to calculate the internal force constants shown in Table S8 (Supporting Information). They are compared with equivalent values for related molecules. As observed, the force constants corresponding to internal coordinates comprising the C(1)—S bond and C(1)-S-S angle in CF$_3$SO$_2$SCH$_3$ have lower and higher values, respectively, than those calculated for the other molecules. This can be explained by the higher anomeric effect, LP S → σ* C (1)–S(2) in the CF$_3$SO$_2$SCH$_3$ molecule.

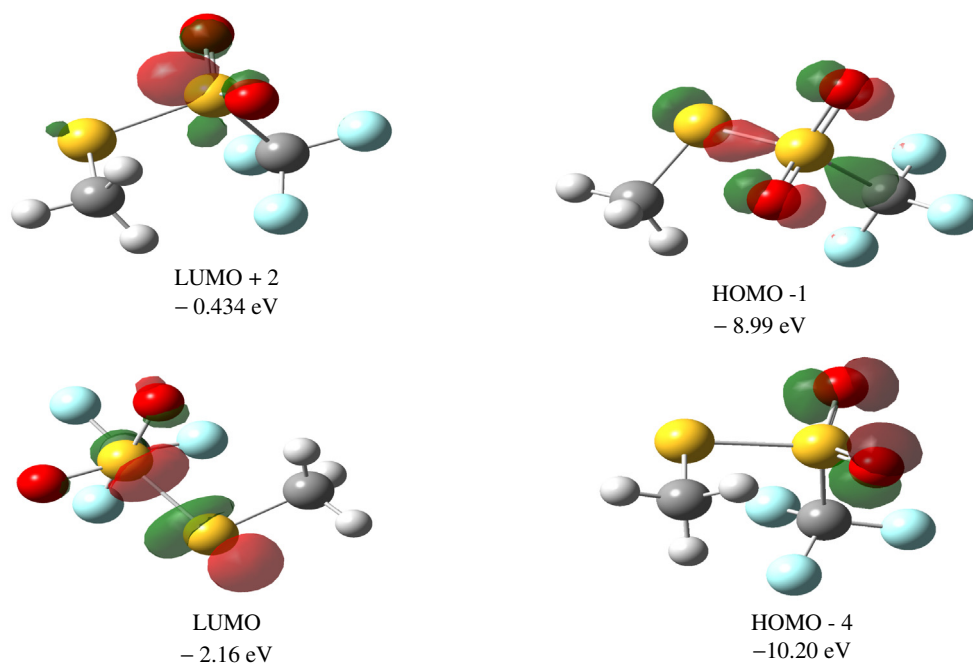LUMO + 2
− 0.434 eV

HOMO -1
− 8.99 eV

LUMO
− 2.16 eV

HOMO - 4
−10.20 eV

Fig. 6. Molecular orbitals involved in the electronic transitions of CF$_3$SO$_2$SCH$_3$ calculated in gas phase. Computed energies are also given.

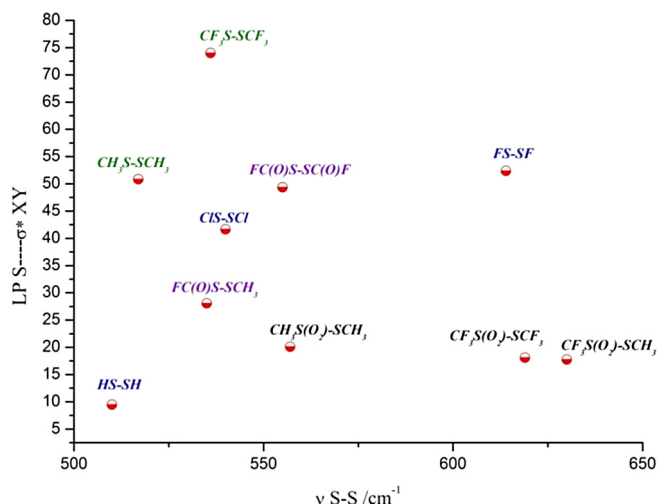**Fig. 7.** Relationship between the anomeric effect LP S → σ*S-S with υS-S in different thio-compounds.

7. Conclusions

CF$_3$SO$_2$SCH$_3$ was synthesized according to the literature with some modifications. The theoretical structure derived by quantum calculations shows this molecule as a single *gauche* conformer having a C—S—S—C dihedral angle of 89°. The comparison of the bond lengths of CF$_3$SO$_2$SCH$_3$, obtained by GED and those predicted by various *ab initio* and DFT methods, shows that CF$_3$SO$_2$SCH$_3$ is a particularly challenging case for theoretical geometry optimization. The inclusion of multiple polarization functions in the basis set plays a crucial role. These results are consistent with common structural features of covalent sulfonates.

The decomposition of the potential-energy function as a Fourier expansion and the analysis of the different (V_i) terms have shown to be useful in analyzing the relative stabilities of different conformations of molecular systems. Since V_2 is the main term of the Fourier expansion, it may be concluded that the hyperconjugative effects, rather than the steric or repulsive interactions, are responsible for the observed composition.

The role of hyperconjugative interactions in the stabilization of the *gauche* form has been assessed by NBO analysis, where the hyperconjugation represents the transfer of one electron from a lone pair or bonding orbital to an antibonding orbital. The S-S bond is very sensitive to electrostatic behavior. For X-SS-X compounds (X = F, Cl, CF$_3$, CH$_3$, FC(O)) it shows that a higher electronegativity of X increases the anomeric effect (S···XY) and, therefore, the value of the υ S-S frequency.

However, this behavior is not observed in thiosulfonates where the presence of the SO$_2$ group causes an increase in the electron density, when the CX$_3$ (X = H, F) groups have different electronegativities and the interacting atoms present a positive charge that favors the anomeric effect (LP S → σ* C (1)–S(2)).

IR and Raman spectra were obtained for CF$_3$SO$_2$SCH$_3$and the vibrational data were used as a basis to define an SQM force field and internal force constants. In covalent sulfonates, the SO$_2$ stretching modes were very sensitive to changes in the electronegativity of the substituents. The increase in the electronegativity of the CX$_3$ group caused a greater separation between the antisymmetric and symmetric stretching bands.

Acknowledgements

Appendix A. Supplementary data

Supplementary data associated with this article can be found, in the online version, at http://dx.doi.org/10.1016/j.ica.2016.10.020.

References

[1] S. Surqui, K. Okamoto, M. Ohnishi, H. Makito, T. Kawamori, T. Watanake, T. Tamaka, Y.K. Nakamura, Y. Nakamura, I. Tomito, H. Mori, J. Cancer Res. 88 (1997) 5.
[2] C. Fahlke, T.H. Rhodes, R.R. Desai, A.L. George Jr., Nature 3948 (1998) 687.
[3] M. St-Vincent, M. Dickman, J. Chem. Educ. 81 (2004) 1048.
[4] H. Mori, K. Matsunaga, Y. Tanakamaru, K. Kawabata, Y. Yamada, S. Sugie, A. Nishikawa, Cancer Lett. 135 (1999) 123.
[5] Y.K. Nakamura, T. Matsuo, K. Simio, Y. Nakamura, I. Tomita, Biochem. 60 (1996) 1439.
[6] P. Jeschke, Pest Manage. Sci. 66 (2010) 10.
[7] M.E. Tuttolomondo, A. Navarro, T. Peña, E.L. Varetti, S.F. Parker, A. Ben, J. Phys. Chem. A 113 (29) (2009) 8401–8408.
[8] M.E. Defonsi Lestard, L.A. Ramos, M.E. Tuttolomondo, S.E. Ulic, Spectrosc. 59 (2012) 40–46.
[9] M.E. Defonsi Lestard, S.B. Díaz, M.E. Tuttolomondo, Spectrochim. Acta Part A 97 (2012) 479–489.
[10] V. Miguel, M.E. Defonsi Lestard, M.E. Tuttolomondo, S.B. Díaz, A. Ben Altabef, M. Puiatti, A.B. Pierini, Biochim. Biophys. Acta 2016 (1858) 38–46.
[11] R.N. Haszeldine, J.M. Kidd, J. Chem. Soc. (1955) 2901.
[12] F. Trautner, A. Ben Altabef, L.E. Fernández, E.L. Varetti, H. Inorg. Chem. 38 (1999) 3051.
[13] M.E. Tuttolomondo, P.E. Argañaraz, E.L. Varetti, S.A. Hayes, D.A. Wann, H.E. Robertson, D.W.H. Rankin, Eur. J. Inorg. Chem. (2007) 1381.
[14] M.E. Tuttolomondo, A. Navarro, T.P.E. Peña, E.L. Varetti, S.A. Hayes, D.A. Wann, H.E. Robertson, D.W.H. Rankin, A. Ben, J. Phys. Chem. A 111 (2007) 9952.
[15] M.J. Frisch, G.W. Trucks, H.B. Schlegel, G.E. Scuseria, M.A. Robb, J.R. Cheeseman, J.A. Montgomery Jr., T. Vreven, K.N. Kudin, J.C. Burant, J.M. Millam, S.S. Iyengar, J. Tomasi, V. Barone, B. Mennucci, M. Cossi, G. Scalmani, N. Rega, G.A. Petersson, H. Nakatsuji, M. Hada, M. Ehara, K. Toyota, R. Fukuda, J. Hasegawa, M. Ishida, T. Nakajima, Y. Honda, O. Kitao, H. Nakai, M. Klene, X. Li, J.E. Knox, H. P. Hratchian, J.B. Cross, V. Bakken, C. Adamo, J. Jaramillo, R. Gomperts, R.E. Stratmann, O. Yazyev, A.J. Austin, R. Cammi, C. Pomelli, J.W. Ochterski, P.Y. Ayala, K. Morokuma, G.A. Voth, P. Salvador, J.J. Dannenberg, V.G. Zakrzewski, S. Dapprich, A.D. Daniels, M.C. Strain, O. Farkas, D.K. Malick, A.D. Rabuck, K. Raghavachari, J.B. Foresman, J.V. Ortiz, Q. Cui, A.G. Baboul, S. Clifford, J. Cioslowski, B.B. Stefanov, G. Liu, A. Liashenko, P. Piskorz, I. Komaromi, R.L. Martin, D.J. Fox, T. Keith, M.A. Al-Laham, C.Y. Peng, A. Nanayakkara, M. Challacombe, P.M.W. Gill, B. Johnson, W. Chen, M.W. Wong, C. Gonzalez, J.A. Pople, Gaussian 03, Revision C.01, Gaussian Inc., Wallingford, CT, 2004.
[16] C. Møller, M.S. Plesset, Phys. Rev. 46 (1934) 618.
[17] W.J. Hehre, R. Ditchfield, J.A. Pople, J. Chem. Phys. 56 (1972) 2257.
[18] P.C. Hariharan, J.A. Pople, Theor. Chim. Acta 28 (1973) 213.
[19] M.S. Gordon, Chem. Phys. Lett. 76 (1980) 163.
[20] A.D. McLean, G.S. Chandler, J. Chem. Phys. 72 (1980) 5639.
[21] R. Krishnan, J.S. Binkley, R. Seeger, J.A. Pople, J. Chem. Phys. 72 (1980) 650.
[22] M.J. Frisch, J.A. Pople, J.S. Binkley, J. Chem. Phys. 80 (1984) 3265.
[23] T.H. Dunning Jr., J. Chem. Phys. 90 (1989) 1007.
[24] A.D. Becke, J. Chem. Phys. 98 (1993) 5648.
[25] C. Lee, W. Yang, R.G. Parr, Phys. Rev. B 37 (1988) 785.
[26] C. Adamo, V. Barone, J. Chem. Phys. 108 (1998) 664.
[27] R.M. Pitzer, W.N. Lipscomb, J. Chem. Phys. 39 (1963) 1995.
[28] E.D., Glendening, J.K. Badenhoop, A.D. Reed, J.E. Carpenter, F.F. Weinhold, Theoretical Chemistry Institute, University of Wisconsin, Madison, WI, 1996.
[29] W.B. Collier, Program FCARTP (QCPE # 631), Department of Chemistry, Oral Roberts University, Tulsa, OK, USA, 1992.
[30] A. Dreuw, M. Head-Gordon, Chem. Rev. 105 (2005) 4009.
[31] M.E. Tuttolomondo, A. Navarro, E.L. Varetti, A. Ben Altabef, Spectrochim. Acta A 61 (2004) 697.
[32] M.E. Tuttolomondo, A. Navarro, E.L. Varetti, A. Ben, J. Raman Spectrosc. 36 (2005) 427.
[33] M.E. Tuttolomondo, L.E. Fernández, A. Navarro, E.L. Varetti, A. Ben, Spectrochim. Acta Part A 60 (2004) 611.
[34] M.E. Defonsi Lestard, L.A. Ramos Guerrero, M.E. Tuttolomondo, S.E. Ulic, A. Ben Altabef, Vib. Spectrosc. 55 (2011) 153.
[35] L. Radom, J.A. Pople, J. Am. Chem. Soc. 92 (1970) 4786.
[36] L. Radom, W.J. Hehre, J.A. Pople, J. Am. Chem. Soc. 94 (1972) 2371.
[37] D. Douglas, J. Org. Chem. 55 (1990) 1003.
[38] S. Millefiori, A. Alparone, J. Chem. Soc. Faraday Trans. 94 (1998) 25.

[39] C.J. Marsden, H. Oberhammer, O. Lösking, H. Willner, J. Mol. Struct. 193 (1989) 233.
[40] C.J. Marsden, B. Beagley, J. Chem. Soc. Faraday Trans. (1981) 77.
[41] C.J. Marsden, B.J. Smith, J. Phys. Chem. 92 (1988) 347.
[42] A. Yokozeki, S.H. Bauer, J. Phys. Chem. 80 (1976) 618.
[43] A. Hermann, S.E. Ulic, C.O. Della Védova, H.G. Mack, H. Oberhammer, J. Fluorine Chem. 112 (2001) 297.
[44] G. Fogarasi, X. Zhou, P.W. Taylor, P. Pulay, J. Am. Chem. Soc. 114 (1992) 8191.
[45] P. Pulay, G. Fogarasi, G. Pongor, J.E. Boggs, A. Vargha, J. Am. Chem. Soc. 105 (1983) 7037.